

How Distance Affects GRB Prompt Emission Measurements

MICHAEL J. MOSS , ^{1,*} AMY Y. LIEN , ² S. BRADLEY CENKO , ^{1,3} SYLVAIN GUIRIC , ^{1,4} AND CRAIG B. MARKWARDT 

¹ *Astrophysics Science Division, NASA Goddard Space Flight Center, Greenbelt, MD 20771, USA*

² *University of Tampa, Department of Chemistry, Biochemistry, and Physics, 401 W. Kennedy Blvd, Tampa, FL 33606, USA*

³ *Joint Space-Science Institute, University of Maryland, College Park, MD 20742, USA*

⁴ *The Department of Physics, The George Washington University, 725 21st NW, Washington, DC 20052, USA*

ABSTRACT

We investigated how Gamma-Ray Burst (GRB) prompt emission measurements are affected by increasing distance to the source. We selected a sample of 26 bright GRBs with measured redshifts $z < 1$ observed by the Burst Alert Telescope (BAT) on board the Neil Gehrels Swift Observatory (Swift) and simulated what BAT would have observed if the GRBs were at larger redshifts. We measured the durations of the simulated gamma-ray signals using a Bayesian block approach and calculated the enclosed fluences and peak fluxes. As expected, we found that almost all durations (fluences) measured for simulated high- z GRBs were shorter (less) than their true durations (energies) due to low signal-to-noise ratio emission becoming completely dominated by background, i.e., the “tip-of-the-iceberg” effect. This effect strongly depends on the profile and intensity of the source light curve. Due to the uniqueness of GRB light curves, there is no common behavior in the evolution of measured durations with redshift. We compared our synthetic high- z (i.e., $z > 3$) GRBs to a sample of 72 observed high- z bursts and found that the two samples were not inconsistent with being drawn from the same underlying population. We conclude that: (i) prompt emission durations (fluences) of high- z GRBs observed by Swift/BAT are most likely underestimations, sometimes by factors of \sim several tens (~ 2), and (ii) changes in the average GRB prompt emission duration and fluence with increasing redshift are consistent with the tip-of-the-iceberg effect.

Keywords: Gamma-Ray Bursts (629)

1. INTRODUCTION

A Gamma-ray Burst (GRB) is characterized by a bright highly-variable flash of gamma-rays that can last for a fraction of a second or tens of seconds, known as prompt emission. This initial phase is followed by a period of decaying emission that can be observed from radio frequencies to TeV energies and that lasts for hours, days, and, occasionally, years, known as afterglow emission. These catastrophic events are the signatures of highly relativistic material being jetted away from a compact object (G. Cavallo & M. J. Rees 1978; M. J. Rees & P. Meszaros 1992) newly formed by either the core-collapse of a massive star (T. J. Galama et al. 1998; J. Hjorth et al. 2003; K. Z. Stanek et al. 2003) or the merger of a compact binary system (N. R. Tanvir et al.

2013; B. P. Abbott et al. 2017). The prompt emission is often associated with particle acceleration and energy dissipation mechanisms occurring within the outflow (B. Zhang 2014), while afterglow emission is often adequately modeled as a decelerating relativistic blast wave continually sweeping up material from the medium surrounding the burst (R. D. Blandford & C. F. McKee 1976; R. A. M. J. Wijers et al. 1997; R. Sari et al. 1998; D. A. Frail et al. 2000).

Due to their incredible luminosities, GRBs can be detected across most of the observable universe. They have been detected from redshifts as low as $z = 0.0085$ (T. J. Galama et al. 1999) and out to $z \sim 9.4$ (T. N. Ukwatta et al. 2009; A. Cucchiara et al. 2011), making them excellent tools to study cosmological aspects of our universe, such as star formation rates (T. Totani 1997; R. A. M. J. Wijers et al. 1998; S. Mao & H. J. Mo 1998; C. Porciani & P. Madau 2001) and the re-ionization phase of the early Universe (J. Miralda-Escudé 1998;

Email: mikejmoss3@gmail.com

* NASA Postdoctoral Fellow

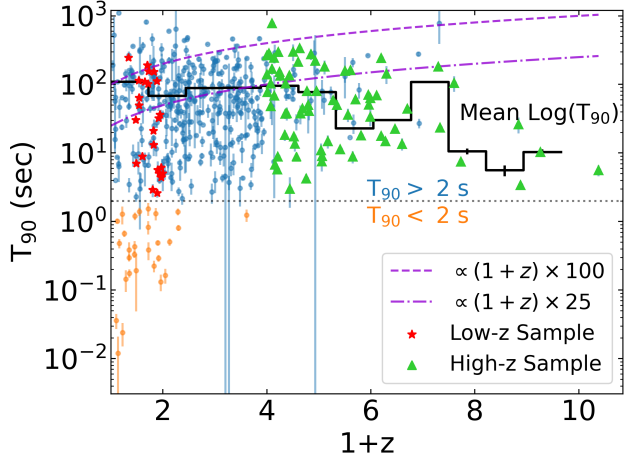


Figure 1. T_{90} measurements of Swift/BAT GRBs as a function of their measured redshifts. The blue and orange points are GRBs with a measured prompt duration of $T_{90} > 2$ s and $T_{90} < 2$ s, i.e., long and short GRBs, respectively. The lower and upper violet dashed lines are $\propto (1+z)T$ for rest frame durations of $T = 25$ s and 100 s, respectively. The black line is the weighted mean of the log durations of LGRBs in each sequential redshift bin, i.e., $\mu = \sum x_i \sigma_i^{-2} / \sum \sigma_i^{-2}$, where $x_i = \log_{10}(T_{90,i})$. The red stars and green triangles indicate GRBs in the low- z and high- z samples of this work, respectively (see Tables 4 and 5).

T. Totani et al. 2006; N. R. Tanvir et al. 2019; H. M. Fausey et al. 2024).

The duration of GRB prompt emission is typically defined using the T_{90} metric, i.e., the time interval which encompasses 5% to 95% of the observed burst count fluence in the 50-300 keV energy band (C. Kouveliotou et al. 1993). By defining the spectral hardness of a GRB as the ratio between the fluence in the 100-300 keV and 50-100 keV energy bands, there is a bimodality in the observed GRB population separated into short-hard GRBs (SGRBs; i.e., $T_{90} < 2$ s and a higher hardness ratio) and long-soft GRBs (LGRBs; i.e., $T_{90} > 2$ s and a lower hardness ratio). Exactly where the separation between the two populations occurs is unclear and has been found to depend on which instrument was used to perform the measurements (O. Bromberg et al. 2012).

The coincidental detections of LGRBs with core-collapse supernova (T. J. Galama et al. 1998; J. Hjorth et al. 2003) and SGRBs with binary-merger events (N. R. Tanvir et al. 2013; B. P. Abbott et al. 2017) have provided a naive explanation for the observed bimodality. However, there is a significant overlap between the durations and hardness ratios of the two populations and several GRBs have called into question the simple association between a GRB's duration and spectral properties with its progenitor system. For example, GRB 200826A

has a $T_{90} \sim 1.14$ s, placing it into the SGRB population, but was later found to have a supernova counterpart (T. Ahumada et al. 2021; A. Rossi et al. 2022), linking it to a collapsar progenitor. Conversely, GRBs 211211A and 230307A were both clearly LGRBs (i.e., $T_{90} \sim 122$ s and 35 s, respectively), but both were associated with counterparts consistent with kilonovae, which are signatures of compact binary mergers (J. C. Rastinejad et al. 2022; E. Troja et al. 2022; A. J. Levan et al. 2024).

Naively, the average measured duration of LGRBs should increase with redshift simply due to time dilation, i.e., $\bar{T}_{90} \propto (1+z)$. However, the average duration of LGRBs seems to remain constant out to high redshifts ($z \sim 7$), at which point the average duration begins to sharply decrease (see Fig. 1).

Low SNR observations lead to underestimations of GRB durations and fluences due purely to instrumental biases; this is known as the “tip-of-the-iceberg” effect (J. T. Bonnell et al. 1997; D. Kocevski & V. Petrosian 2013; O. M. Littlejohns et al. 2013; M. Moss et al. 2022; M. Llamas Lanza et al. 2024). Low SNR observations can be caused by either the observing conditions during an observation (e.g., background level and incident angle of the source relative to the detector plane; M. Moss et al. 2022; M. Llamas Lanza et al. 2024) or the physical conditions of the source itself (e.g., intrinsic brightness and distance; J. T. Bonnell et al. 1997; D. Kocevski & V. Petrosian 2013; O. M. Littlejohns et al. 2013; M. Llamas Lanza et al. 2024). Furthermore, the duration of GRB prompt emission is energy dependent. Higher energy emission is typically shorter than the emission at lower energies (E. E. Fenimore et al. 1995). As the distance to a GRB increases, the rest-frame spectra is redshifted such that higher energy parts of the intrinsic GRB spectrum will fall in the instrument energy band, meaning we should expect the duration of high-redshift GRBs to be shorter.

J. T. Bonnell et al. (1997) compared the duration measurements of bright GRBs detected by the *Burst And Transient Source Experiment* on board the Compton Gamma-Ray Observatory (CGRO/BATSE) and found that a brightness bias exists for GRB duration measurements. This bias was sufficient to obscure a time-dilation factor of order ~ 2 . D. Kocevski & V. Petrosian (2013) simulated a set of synthetic Fast-Rise Exponential-Decay (FRED) light curves each with different brightnesses at increasing distances, folded them through the instrument response matrix of CGRO/BATSE, added background signal, and then measured their durations. The authors found that at lower redshifts, the burst durations evolved as $\propto (1+z)$, however, at higher redshifts the burst durations stopped

following this trend and began to decrease due to decreasing signal-to-noise ratios (SNRs). O. M. Littlejohns et al. (2013) took a sample of low-redshift bursts observed by Swift/BAT and simulated the burst light curves at higher redshifts with the purpose of comparing the durations measured for the simulated bursts to the durations measured for the farthest GRBs observed by Swift/BAT. The authors found that their simulated light curves had average duration measurements higher than the average duration of the observed high-redshift bursts by a factor $\gtrsim 3$ and that the duration measurement distribution between the two samples only had a $\sim 1\%$ probability of being consistent with being drawn from the same underlying population.

In this work, we further investigated the tip-of-the-iceberg effect to understand how duration and fluence estimates for GRB prompt emission observed by Swift/BAT evolve with redshift, expanding upon previous studies by taking into account proper distance corrections and folding observed spectra with the instrument response of Swift/BAT to properly account for signal loss due to instrument sensitivity. In Section 2, we outline the procedures and methods we used to simulate Swift/BAT observations of GRBs. In Section 3, we display our results with discussion in Section 4. We conclude in Section 5. Throughout this work we assume typical parameter values for standard Λ CDM cosmology models, i.e., $\Omega_m = 0.3$, $\Omega_\Lambda = 0.7$, and $H_0 = 67.4 \text{ km s}^{-1} \text{ Mpc}^{-1}$ (Planck Collaboration et al. 2020).

2. METHODS

Our goal was to study how the distance to a GRB impacts the duration and fluences estimated for Swift/BAT observations. To do this, we selected a sample of GRBs observed with Swift/BAT at low redshift ($z < 1$) and simulated them at increasing distances up to $z = 15$ or until the bursts could no longer be detected by Swift/BAT. We used the Bayesian block algorithm to estimate the T_{90} and fluences of the simulated bursts and compared these results to the input burst parameters to assess the impact of the distance to the source. All simulations in this work were completed using the publicly available `simmes` package⁵. Finally, we compared the measurements of our simulated bursts to a sample of GRBs observed with Swift/BAT at redshifts of $z \geq 3$. A schematic of the methodology used in this work is shown in Figure 2.

We compiled our sample of GRBs by first selecting bursts observed by Swift/BAT (S. D. Barthelmy et al. 2005) between December 2004 - June 2025 that

had redshift measurements. The automated analysis of Swift/BAT GRBs includes a spectral fit to the 1-second peak flux emission in the 15-150 keV range using both power law and cut-off power law models. For the GRBs in our sample, we assume their spectra are well represented by the best-fit cut-off power law⁶ (CPL), regardless of whether the automated analysis preferred a power law or CPL. We required each burst to have a CPL peak energy to be $E_p \leq 550 \text{ keV}$. This removed any bursts with unconstrained peak energies far outside the BAT energy band⁷.

Typically, GRB spectra peak at lower energies near the start and end of the burst emission. Therefore, using time-resolved spectra in our simulations generally lead to burst signals being lost into the background noise faster than when using a single time-integrated spectra. We found that using time-resolved spectra did not lead to significant changes in our final interpretations, but can increase computation time significantly. Therefore, we decided to use the best-fit 1-second peak spectral model found for each burst as the spectrum across the entire burst interval. As a result, our estimations on the loss of burst signal are conservative.

Lastly, we applied a distance-dependent peak-flux cut by assuming a mock peak flux value at $z = 3$ and calculating what the peak flux would be as a function of redshifts (see Eq. 1 below) and for a range of spectral shapes (i.e., assuming a CPL spectrum defined as $dN/dE = N_0(E/50. \text{ keV})^\alpha e^{-E(2+\alpha)/E_p}$, where the photon index ranged from $\alpha = -1.5$ to -0.5 , peak energies ranged from 50 to 550 keV, and $N_0 = 1$ is the flux normalization). The peak flux value we assumed is equal to twice the theoretical Bayesian block sensitivity limit, A , given by $A = \bar{\sigma} \Delta t \sqrt{2 \log n}$ (J. D. Scargle et al. 2013), where $\bar{\sigma}$ is average background variance of BAT mask-weighted light curves (see Fig 4), Δt is the time bin size, and n is the number of bins in the light curve. We assume $\Delta t = 1 \text{ sec}$ and $n = 50$. This flux value was extrapolated to all redshifts between $z = 0 - 10$ assuming spectral defined by $dN/dE \propto (E/50. \text{ keV})^\alpha e^{-E(2+\alpha)/E_p}$, where the photon index was varied between $\alpha = -1.5$ to -0.5 and peak energies varied between from 50 to 550 keV. This flux cut ensured that each burst in our sam-

⁶ A spectrum with a peak energy is required so that the total energy of a simulated GRB does not tend toward infinity as it is simulated out to increasing redshifts.

⁷ Since these bursts will be used as mock GRBs for our simulations, we do not require the peak energies to be strongly constrained measurements, only that they are in reasonable agreement with measurements made for the entire GRB population

⁵ <https://github.com/mikemoss3/simmes>

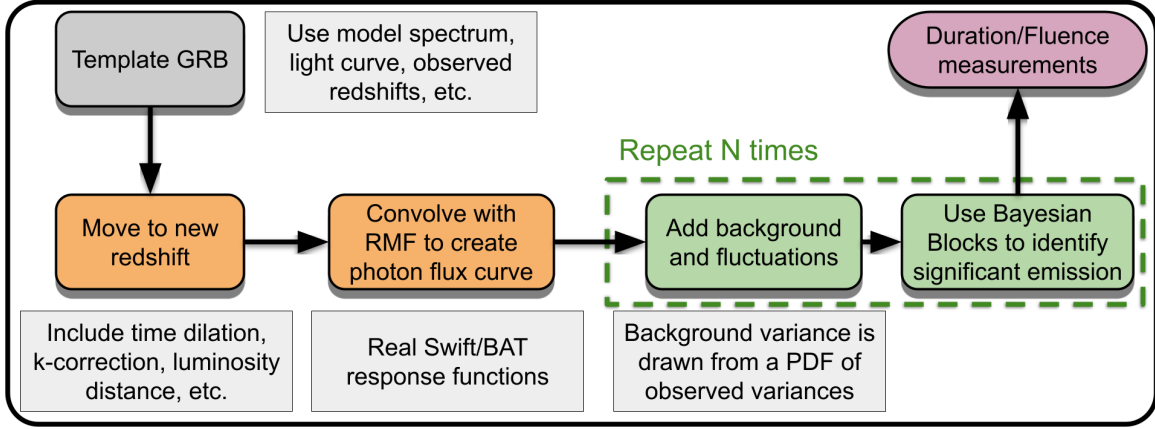


Figure 2. Work flow schematic of the simulations and measurements performed in this work.

ple would be measurable out to at least $z = 3$ (see yellow region in Fig. 3).

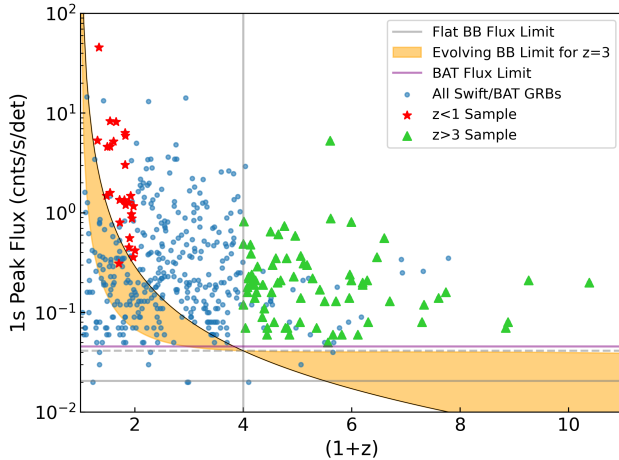


Figure 3. Peak flux measurements of Swift/BAT GRBs as a function of their measured redshifts. Blue points are all Swift/BAT GRBs. The red stars and green triangles indicate GRBs in the low- z and high- z samples of this work, respectively (see Tables 4 and 5). The horizontal gray line indicates the theoretical Bayesian block sensitivity limit, the dashed line is twice that limit (see text for details). For reference, the horizontal purple line indicates the BAT flux sensitivity assuming a 1 second exposure (W. H. Baumgartner et al. 2013; A. Lien et al. 2016). The thin black line represents a 1s peak flux value equal to twice Bayesian block sensitivity limit at $z = 3$ calculated at other redshifts between $z = 0-10$ assuming a spectrum $dN/dE \propto (E/50. \text{ keV})^\alpha e^{-E(2+\alpha)/E_p}$, where the photon index is assumed to be $\alpha = -1.5$ and the peak energy to be $E_p = 50 \text{ keV}$. The region shaded in yellow defines the same extrapolated flux value but assuming different spectral shapes (see text for details).

We then separated the observed sample into low- z GRBs (i.e., 26 GRBs with $z < 1$; see red stars in Fig. 1 and 3) and high- z GRBs (i.e., 72 GRBs with $z > 3$;

see green triangles in Fig. 1 and 3). Tables 4 and 5 in Appendix B list the GRBs included in this work. We now describe how the observed low- z GRBs were simulated out to higher redshifts and then compared to the observed high- z sample.

For each GRB in our low- z sample, we download the observed Swift/BAT mask-weighted 15 - 350 keV light curve⁸ and best-fit spectral model parameters⁹. For bursts in our sample with $T_{90} \leq 10 \text{ sec}$, we used 64 ms time binned light curves and 1 second time binned light curves for bursts with $T_{90} > 10 \text{ sec}$. Because we assumed the burst spectrum is equal to the best-fit spectrum model found for the 1-second peak interval, we normalized the light curves by the fluence within the 1-second peak interval, leaving us with a dimensionless light curve that realistically mimics GRB light curve behavior. We did not apply any smoothing to the light curves. These normalized light curves were used to indicate the relative fluxes in each bin while the best-fit spectral model were used to determine the actual count rates in each bin. For each light curve, we isolate the burst signal and remove background by omitting any signal outside of the estimated T_{100} ¹⁰.

We simulated GRBs at higher redshifts by taking into account the cosmological effects on the observed light curve profile and spectra (i.e., time dilation, k correction, luminosity distance). A burst observed in the energy band $[e_1, e_2]$ at a redshift z_1 with a measured flux $F_{z_1, [e_1, e_2]}$ and spectrum $\phi_1(E)$ will have a **flux** given by

⁸ Mask-weighting is a standard procedure for coded-mask aperture instruments such as Swift/BAT (S. D. Barthelmy et al. 2005; J. DeLaunay & A. Tohuvavohu 2022).

⁹ See automated GRB data products at <https://swift.gsfc.nasa.gov/results/batgrbcat/>

¹⁰ In addition to the T_{90} , the Swift/BAT team reports the duration which encompasses 100% of the significantly detected burst emission, i.e., the T_{100} .

$$F_{z_2,[e_1,e_2]} = \frac{D_{L,z_1}^2(1+z_2)}{D_{L,z_2}^2(1+z_1)} F_{z_1,[e_1,e_2]} \times \frac{k[e_1, e_2, E_1, E_2, z_1, \phi_{z_1}(E)]}{k[e_1, e_2, E_1, E_2, z_2, \phi_{z_2}(E)]} \quad (1)$$

if it were instead at z_2 , where $\phi_{z_2}(E)$ is the spectrum that would be observed at z_2 , D_{L,z_i} is the luminosity distance at a redshift z_i , and $[E_1, E_2] = [0.1, 10, 000]$ keV adequately approximates the bolometric energy band. For this work, we use the complete Swift/BAT energy band, i.e., $[e_1, e_2] = [15, 350]$ keV. $k[e_1, e_2, E_1, E_2, z, \phi(E)]$ is the k -correction factor that occurs as the observed spectra is redshifted into the observing band (J. S. Bloom et al. 2001),

$$k[e_1, e_2, E_1, E_2, z, \phi(E)] = \frac{F_{[E_1/(1+z), E_2/(1+z)]}}{F_{[e_1, e_2]}} \quad (2)$$

$$= \frac{\int_{E_1/(1+z)}^{E_2/(1+z)} E \phi(E) dE}{\int_{e_1}^{e_2} E \phi(E) dE}, \quad (3)$$

The redshifted spectra (units photons / s / keV / cm²) are then convolved with the Swift/BAT instrument response function to produce mock folded spectra (units counts / sec / keV / on-axis fully-illuminated detector¹¹). For this work, we assumed that all simulated bursts were observed on-axis compared to the detector bore-sight (i.e., $\theta_{\text{inc}} = 0$ and PCODE=1, where PCODE is the partial coding fraction which defines the average fraction of each detector illuminated by a source through the coded mask accounting for both the source incident angle and instrument geometry). Furthermore, we assumed that all 32,768 detectors on the Swift/BAT detector plane were enabled during each mock observation. We found that we needed to scale the folded spectra by a factor of 2 to ensure that the simulations would remain self consistent with the input observations. Taking the integral of the folded spectra across the most-sensitive interval of the BAT energy band (i.e., 15 - 150 keV) gave an observed count flux (units of counts / sec / on-axis fully-illuminated detector), which differs from the emitted count flux due to instrumental effects and sensitivity. We then multiplied the normalized light curves by their respective observed count fluxes to obtain mock Swift/BAT mask-weighted light curves for each burst.

Mask-weighted light curves are inherently background subtracted, meaning that outside of any source emis-

sion interval the average count rate will be ~ 0 cnts/s. The fluctuations around zero are determined by the raw background count rate during observation (e.g., a larger raw background count level leads to larger variations in the mask-weighted light curve). To mimic these background fluctuations, we compiled a distribution of 1-second time-bin background variances for all GRBs observed with Swift/BAT (see Fig. 4) and fit a FRED function (D. Kocevski et al. 2003) to the distribution to create a probability distribution function (PDF). For each simulation, we randomly selected a background variance value from this PDF and then added mock background fluctuations to the light curve.

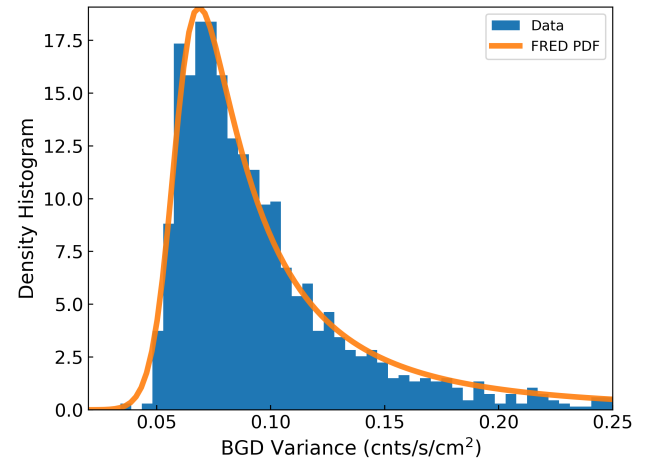


Figure 4. We compiled the 1-second time-bin background variances from the mask-weighted light curves of all Swift/BAT GRBs (blue) and fit a FRED function to the distribution to create a probability distribution function (orange). The background variances were calculated within the 50 second intervals preceding and following the emission of each burst. We sampled this distribution during our simulations to determine the background variance of each simulated light curve.

Finally, the mock mask-weighted light curves were passed through a Bayesian-block algorithm¹² to obtain duration measurements (J. D. Scargle et al. 2013). For this work, we did not use the Swift/BAT trigger algorithms to trigger on simulated light curves and, instead, directly applied the Bayesian block algorithm to obtain duration measurements. This methodology is more similar to ground-based analyses of Swift/BAT data when searching for sub-threshold bursts. The Bayesian-block algorithm is sensitive to the duration of the background interval it uses to test for significant emission. However,

¹¹ The unit “on-axis fully-illuminated detector” is unique to coded-mask aperture instruments, a definition of what each term signifies can be found here: <https://swift.gsfc.nasa.gov/analysis/thread/batfluxunit/thread.html>

¹² https://docs.astropy.org/en/stable/api/astropy.stats.bayesian_blocks.html

increasing the light curve length also increases Bayesian block computation time. For that reason, when we added mock background emission, we use a background interval that was at least $\geq T_{100}$ onto either side of the source emission interval.

For every burst in our low- z sample, we simulated the burst across 50 different redshifts, starting at the burst's observed redshift and increase to $z = 15$ or until the burst was no longer measurable using the Bayesian-block algorithm. We simulate mock GRBs 1000 times at each redshift, varying the count flux for each simulation as described above.

3. IMPACT OF DISTANCE ON GRB MEASUREMENTS

To illustrate the tip-of-the-iceberg effect, we show an example GRB 140512A simulated at different redshifts in Figure 5. At the burst's observed redshift, $z = 0.725$, the light curve shows multiple pulses of varying brightnesses lasting for $T_{90,\text{rest}} \sim 154$ sec. When the burst is moved to $z = 3$, only two dim pulses separated by a quiescent period are visible for a total duration of $T_{90} \sim 329$ sec. In this case, the early emission episode may even be interpreted as a GRB precursor (T. Murakami et al. 1991; T. M. Koshut et al. 1995; E. Troja et al. 2010). At $z = 6$, only the main emission period remains significant above background and the duration becomes $T_{90} \sim 157$ sec, similar to the duration measured at $z = 0.725$.

In Figure 6, we show the simulation results for GRB 050525A, a burst with an observed light curve that exhibits two bright and well-defined FRED pulses with a measured duration of $T_{90,\text{rest}} = 8.836$ sec. The durations and fluences measured for all simulations are displayed in the two density plots and show how the T_{90} and fluence measured for the simulations evolve with redshift. As the redshift increases from the measured redshift $z = 0.61$ out to higher redshifts, the measured durations stay proportional to $\propto T_{90,\text{rest}} \times (1 + z)$. However, above $z \sim 8$, duration measurements begin to drop far below the expected time-dilation line, indicating that the tip-of-the-iceberg effect is starting to have an effect on the duration measurements. Duration measurements above $T_{90,\text{rest}} \times (1 + z)$ are purely due to random fluctuations in the background noise. The fluence measurements are proportional to $\propto k(z)/D_L^2(z)$ but quickly become underestimates of the intrinsic fluence.

Another example of our simulation results is shown for GRB 111228A in Figure 7. Starting at $z \sim 2$ the duration measurements begin to have a bimodal or even a trimodal distribution. This behavior occurs when the dimmer pulses at the beginning and end of GRB 111228A become so dim they are no longer significant above back-

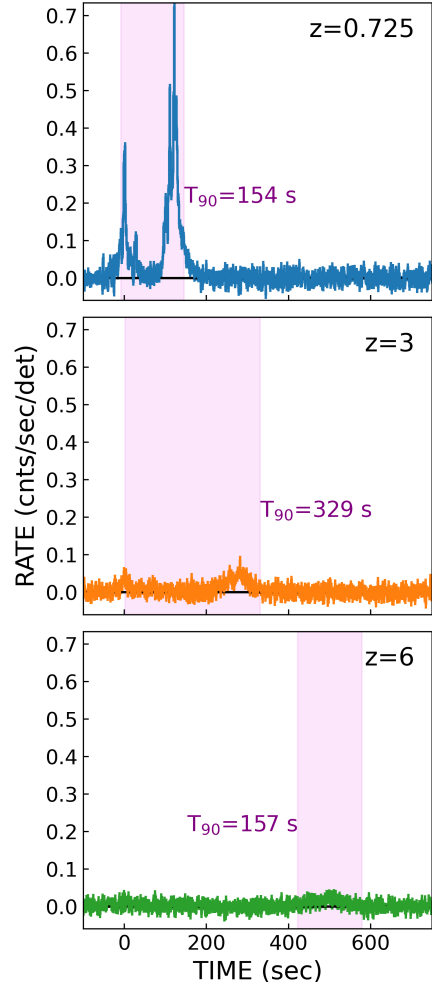


Figure 5. *Top:* The light curve of GRB 140512A, observed at a redshift of $z = 0.725$, displays multiple pulses of emission ($T_{100} \sim 154$ seconds). Shaded regions indicate the measured T_{90} . *Center and Bottom:* Using our simulation tool, we show what the same light curve looks like when shifted to $z = 3$ and $z = 6$, respectively. With increasing redshift, the luminosity of the burst is decreased and the signal is stretched due to time dilation. At $z = 3$, the early time emission is still visible and could be interpreted as a precursor. At $z = 6$, only the main emission period remains significant for Swift/BAT.

ground and, therefore, are not included in the duration estimate found by the Bayesian block algorithm. At $z \sim 2$, GRB 111228A would have had an equally likely chance to have a measured duration of ~ 175 sec and ~ 75 sec. Depending on the structure of the input light curve, it is common to see such abrupt jumps or discontinuities in the evolution of the T_{90} measurements. However, these abrupt changes in T_{90} measurements are not necessarily present in the measured fluence, since the

majority of the fluence is within the brightest pulse(s) of the light curve.

Once source signal becomes dim enough that it is no longer distinguishable from background noise it becomes unrecoverable without prior knowledge of the underlying light curve. And since prompt emission light curves of GRBs vary so strongly between bursts, there is no common behavior in the evolution of the measured durations with increasing redshift. However, for every GRB in our sample, duration measurements at higher redshifts significantly underestimated the time-dilation corrected duration, indicating that the tip-of-the-iceberg effect plays a significant role in the measured duration of the simulated light curves. Furthermore, some similar features occurred in the duration measurement evolution of several bursts due to similarities in their light curve profiles, e.g., dim pulses towards the beginning or end of the emission interval may lead to disconnected regions of probable duration measurements, as was the case for GRB 111228A.

In some cases, the measured durations seem to show a trend of rising above $T = (1 + z)T_{\text{rest}}$ more than just random fluctuations would cause, e.g., see the measurements for GRB 111228A that rise above the $(1 + z)$ line at $z \sim 5$ (see Fig. 7). This behavior isn't possible in simple analytical cases, but can occur when GRBs have dim pulses or tails of emission on either side of their main emission period that were not completely included in the original T_{90} interval (since the first 5% and last 95% are not included). With increasing redshift, the signal-to-noise ratio of both the main emission period and the dim pulses decrease but, occasionally, background fluctuations will make the dim signal significant enough that it becomes measurable by the Bayesian block algorithm again, and leads to a duration measurement higher than expected. Considering the light curve of GRB 111228A, the emission that occurs between -20 to 0 seconds will become dimmer at higher redshifts, but will occasionally become significant enough to be included in the T_{90} measurements due to background fluctuations, leading to a T_{90} measurement rising above the $(1 + z)$ line. The complete figure set including the input light curves and simulation results for the remaining power law and cut-off power law models GRBs in our low- z sample (24 figures) is available in the online version of the article.

3.1. Long then Short GRBs

In some cases, we found that long GRBs could be measured as short GRBs had they been at higher redshifts (e.g., see GRB 050525 in Fig. 6). GRB 120311A is not

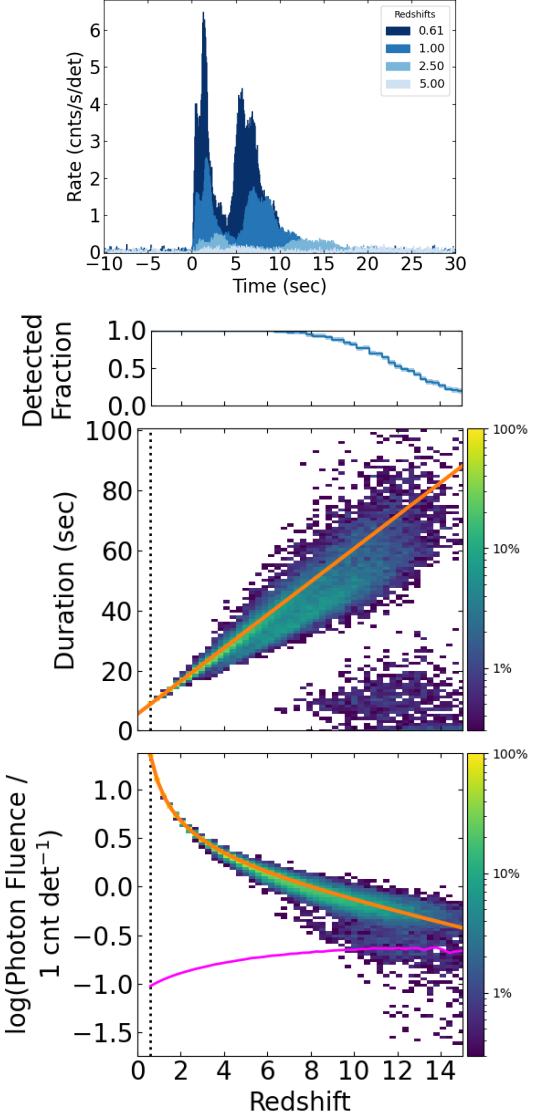


Figure 6. *a:* The 15 - 150 keV Light curve of GRB 050525A simulated at increasing redshifts (indicated by lighter shades of blue). *b:* The fraction of simulations able to be measured by the Bayesian block algorithm in each redshift bin (1,000 simulations were performed in each z bin). *c:* Density plot of the measured T_{90} at increasing redshifts for mock GRBs generated from GRB 050525A data. The black dotted line indicates the measured redshift of the burst, $z_{\text{obs}} = 0.61$. The orange line indicates $\propto T_{90} \times (1 + z) / (1 + z_{\text{obs}})$. Bins with < 3 detections were excluded to remove false positives. *d:* Density plot of the measured fluence as a function of increasing redshift. The orange line indicates the analytically expected fluence, i.e., $\propto k(z) / D_L^2(z)$. The magenta line indicates the Bayesian block detection threshold defined $A = \sigma \sqrt{2 \log(N) T}$ (see text for parameter definitions). The top and bottom color bars indicate the percentage of simulations performed at the same redshift that obtain the same T_{90} or fluence measurement, respectively.

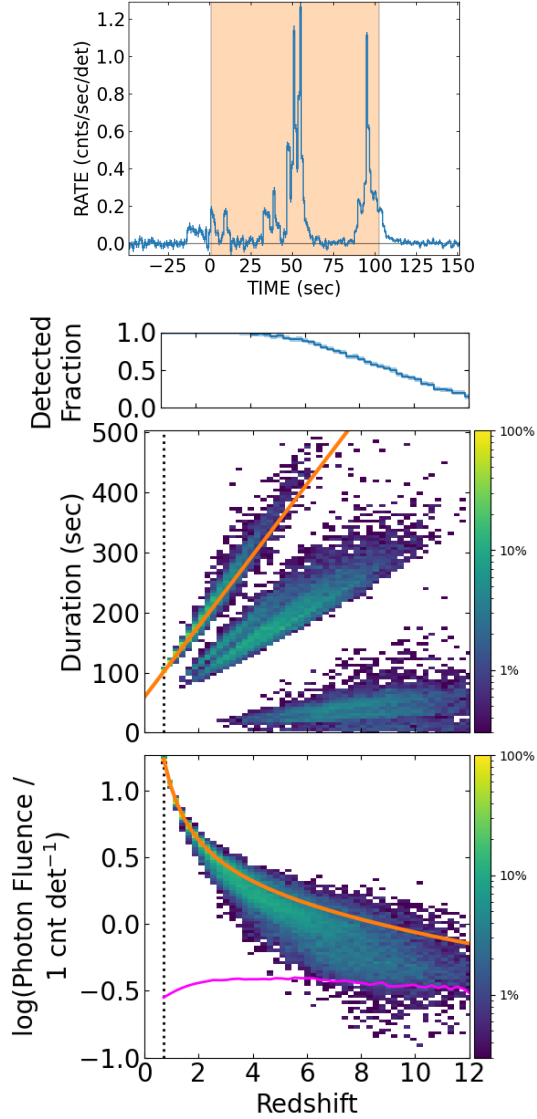


Figure 7. *a:* The 15 - 150 keV light curve for GRB 111228A. The orange shaded region indicates the T_{90} measured by the automated BAT analysis pipeline. Panels *b*, *c*, and *d* are described in Figure 6. The complex multi-pulsed light curve of GRB 111228A leads to discontinuities in the T_{90} evolution. At a redshift of ~ 3 , this burst could have had a measured $T_{90} \approx 20$ sec, an order of magnitude shorter than the true signal duration. The fluence evolution does not show the same strong discontinuities because a majority of the fluence occurs during the brightest pulse. Figures of the simulation results for the remaining GRBs in our low- z sample (24 figures) are available in the online version of the article.

part of our low- z sample, however we simulated it as an exemplary case of this long-to-short behavior. GRB 120311A has a measured redshift of $z = 0.35$ (J. Selsing et al. 2019) displaying a FRED-like light curve with

a $T_{90} = 3.480$ sec. The spectrum of GRB 120311A observed by Swift/BAT was best fit by a power law model (with spectral index $\alpha = -2.176$ and normalization $N_0 = 0.0197$ cnts s^{-1} cm^{-2} keV^{-1}) and, furthermore, was not observed by other gamma-ray instruments, such as Konus instrument onboard the Wind observatory or the Gamma-ray Burst Monitor onboard the *Fermi* Gamma-ray Space Telescope, so we could not constrain the peak energy for a cut-off power-law spectral model. For our simulations, we assumed the measured spectral index and normalization and a peak energy of 550 keV, typical for short-hard GRBs. From our simulations, we found that even at the burst's observed redshift, $z = 0.35$, by simply varying the background, the T_{90} measurement for this burst can change to values ranging from $1 \lesssim T_{90} \lesssim 7$ sec. This is due to the dim tail in the FRED-like pulse of the light curve as parts of the tail become more or less significant above background due to noise fluctuations. However, if instead this burst was observed at a redshift of $z = 0.7$, we would most likely have measured a $T_{90} \sim 1$ sec (see Fig. 8).

We have found that this phenomenon is possible, but does not happen commonly for our sample. It is much more common that a long GRB will fade completely into the noise and become undetectable before becoming a short GRB. However, the sample of bursts we simulated is small compared to the total number of GRBs and, furthermore, selected with criteria in mind to create a bright sample of bursts that could be comparable to high- z bursts. A study on how frequently GRBs with intrinsic durations > 2 sec are observed as SGRBs with $T_{90} < 2$ sec must include a much larger sample of GRBs, including those with unique light curve structures like extended emission, and will be completed in future work.

4. COMPARING OBSERVED AND SIMULATED HIGH- z GRBS

In the top panels of Figure 9 we display the T_{90} , fluence, and 1s peak flux cumulative probability distributions for the observed high- z sample (solid, blue) and the simulated high- z sample (dashed, orange). To test the compatibility of our simulations with the observations we randomly selected 73 simulation results from our entire sample of high- z simulations (i.e., 73 being the same number of bursts in our observed high- z sample) to create 1,000 subsamples. These subsample distributions were used to generate the orange shaded regions in the top panels of Figure 9. We performed a two-sample Kolmogorov-Smirnov test (KS-test) between each subsample and the observed high- z bursts. The cumulative

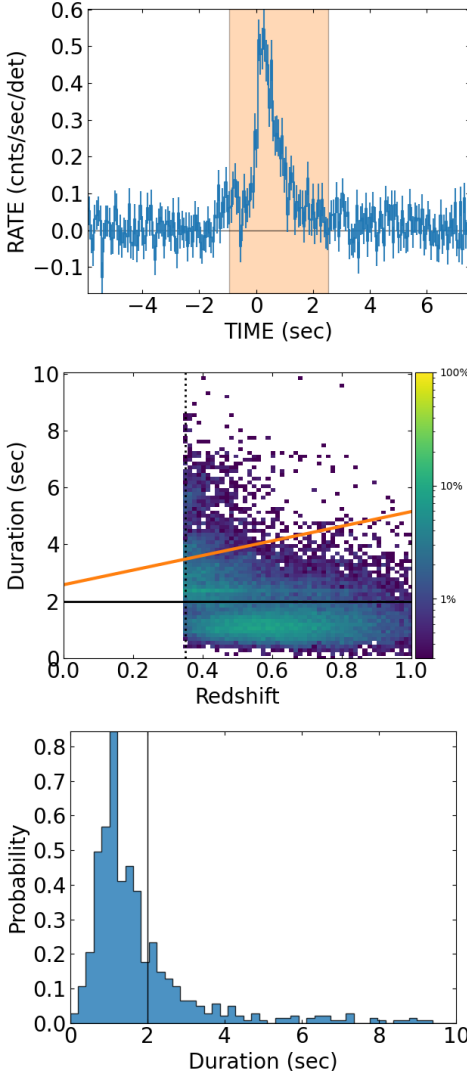


Figure 8. *Top:* The 15 - 150 keV light curve for GRB 120311A as observed by Swift/BAT. The orange shaded region indicates the T_{90} measured by the automated BAT analysis pipeline. *Middle:* Same description as Figure 6b, but for simulations using GRB 120311A as the input GRB. The horizontal, black line indicates the traditional separation between long and short GRBs (i.e., 2 seconds). This is an example of a long GRB becoming a short GRB, simply due to observational bias. *Bottom:* A slice of the duration measurements for GRB 120311A at $z \sim 0.7$.

distributions of the KS-test p -values are displayed in the bottom panels of Figure 9. We find that when comparing the durations of the two samples, 52.2% (99.6%) of p -values are above 0.32 (0.003), indicating that 52.2% (99.6%) of the random subsamples are within 1σ (3σ) of the observed distribution. Similarly, when comparing the fluence distributions, 29.4% (99.4%) of p -values are found to be greater than 0.32 (0.003). However, when we compared the peak-flux distributions, we find

Table 1. Percentage of KS-Test p -values calculated between the high- z simulation subsamples and all observed high- z GRBs that fall within 1, 2, or 3σ

Metric	1σ	2σ	3σ
Durations	52.2%	90.4%	99.6%
Fluences	29.4%	75.8%	99.4%
Peak Flux	0.0%	1.2%	28.4%

Table 2. Percentage of KS-Test p -values calculated between the high- z simulation subsamples and high- z GRBs observed before 2012 that fall within 1, 2, or 3σ

Metric	1σ	2σ	3σ
Durations	75.9%	98.3%	100%
Fluences	74.8%	97.5%	100%
Peak Fluxes	15.3%	54.0%	94.1%

no random subsamples are within 1σ of the observed distribution and only 28.4% are within 3σ (see Tab. 1).

If only the durations of the samples are compared, the simulations and the observations are not incompatible with being drawn from the same underlying distribution (i.e., we cannot reject the null hypothesis of the KS-test) whether a 1, 2, or 3σ agreement threshold is used. When comparing the fluence measurements, a 2, or 3σ threshold still leads to the same conclusion. However, the peak-flux distributions of the two samples appear to differ significantly, both in shape (see Fig. 9 *Bottom Right*) and according to the p -value distribution (see Tab. 1), implying that they were not drawn from the same underlying distribution. On average, the peak fluxes of the observed GRB sample are higher than simulations.

Motivated by the agreement between the duration and fluence measurements, we investigated whether there may be some bias that has arisen in Swift/BAT GRBs over the mission’s lifetime. Splitting the observed sample in roughly half leads to 39 GRBs observed before 2012-01-01 ($\sim 35\%$ of the mission’s life at the time of this publication) and 33 GRBs observed after. In Appendix A, we discuss possible indications that there may

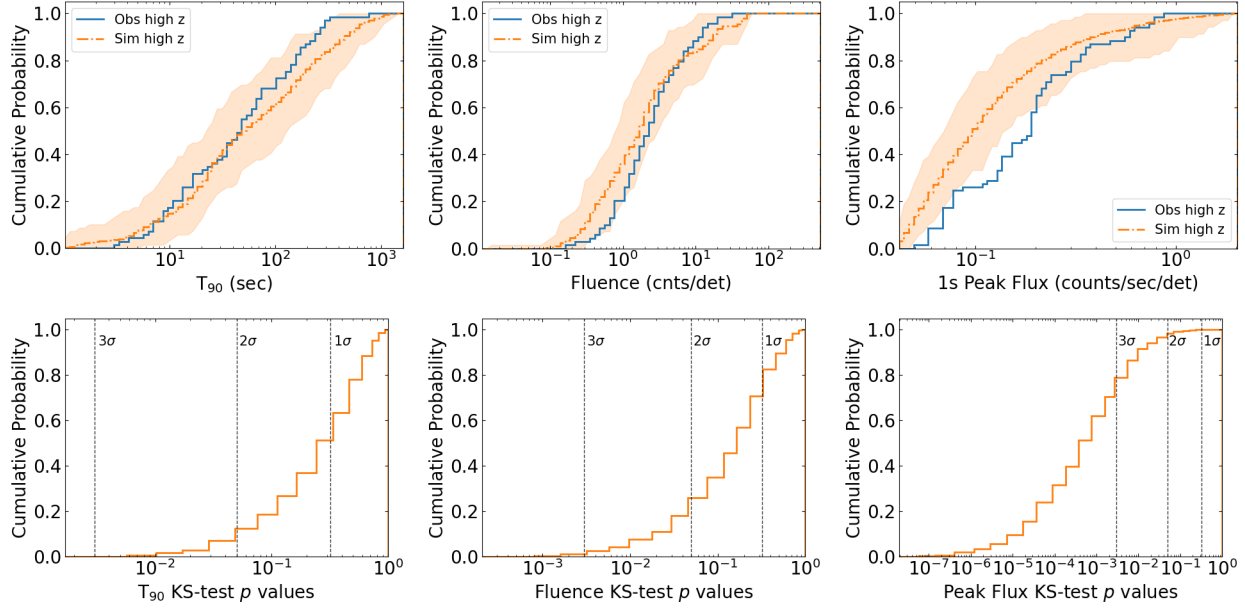


Figure 9. *Top Row:* Cumulative distributions of the T_{90} (left), fluence (center), and peak flux (right) measurements for the observed high- z sample (solid, blue) and the simulated high- z sample (dashed orange). The orange shaded regions indicate the range of cumulative distributions generated from 1,000 trials of randomly sampling 73 simulation results from our entire simulated high- z sample (i.e., the same number as in our observed high- z sample). *Bottom Row:* Cumulative distributions of KS-test p -values calculated between the 1,000 randomly-drawn simulation-subsample distributions and the observed distributions. The vertical dashed lines indicate 1, 2, and 3 σ cut-offs.

be an evolving bias in Swift/BAT GRBs and possible explanations.

The pre-2012 observations and simulation measurements are in a much stronger agreement than the total observed sample (see Fig. 10 and Tab. 2). Both the duration and fluence distributions find $\sim 75\%$ of the random subsamples to be within 1σ of the pre-2012 observations. The peak-flux measurements have also become more consistent, i.e., 15% (94.1%) of the random subsamples are within 1σ (3σ). The agreement between the distributions across each metric implies that the pre-2012 GRB measurements and our mock GRB measurements are not inconsistent with coming from the same underlying distributions.

One possible source of this difference is our requirement that all bursts in both the low- z and high- z samples have observed peak energies constrained to be $E_p \leq 550$ keV. For a burst at a redshift of $z = 0.1$, this observational limit would correspond to a rest-frame $E_{p,0} = 605$ keV, while for a burst at $z = 6$, this would correspond to $E_{p,0} = 3,850$ keV. According to the empirical Yonetoku relation, there exists a positive relation between a GRB's observed luminosity and its peak energy (D. Yonetoku et al. 2004). So, because of the observer-frame E_p limit, our simulated high- z sample will likely have lower peak energies and, therefore, possibly have lower luminosities compared to the observed

high- z sample (which is demonstrated in Fig. 9 *Top Right*). However, this effect is not time dependent and cannot explain why the simulations are in such stronger agreement with the pre-2012 sample of observed bursts than the post-2012 sample.

The fact that the low- z and pre-2012 high- z samples are consistent simply by taking into account cosmological effects and proper observational biases indicates that (i) the significant underestimations of duration and fluence measurements at high z that are found in the simulations should also be assumed to exist in observed high- z GRBs and (ii) no additional physics is needed to explain differences in low- z and high- z GRB prompt duration and fluence measurements.

Since we find that the tip-of-the-iceberg effect leads to dim emission becoming undetectable for our mock GRBs located at high redshifts, we should also expect high- z GRBs to experience the same effect. Consequently, we should not expect the average durations of GRBs to evolve exactly according to cosmological effects. These findings are in agreement with the observed average durations of Swift/BAT GRBs (see Fig. 1). Furthermore, in some cases we found that the measured burst fluence was a factor $\gtrsim 2$ lower than expected from simple distance corrections. These differences imply there may be a systematic error when estimating the isotropic gamma-ray energy values, $E_{\gamma, \text{iso}}$, of GRBs and the dis-

tribution of $E_{\gamma, \text{iso}}$ may extend to higher energies than previously thought (D. Kocevski & N. Butler 2008).

5. CONCLUSION

In this work, we took a sample of bright GRBs observed at redshifts $z < 1$ and simulated them out to $z > 3$. We then compared these simulated GRBs to a sample of GRBs observed at $z > 3$. From this work we found that:

1. due to the tip-of-the-iceberg effect, the duration and fluence measurements of the simulated GRBs are underestimations of their true durations. Sometimes leading to T_{90} measurements that are an order of magnitude below the intrinsic duration.
2. This bias is also true for fluence measurements to a lesser degree, but can be up to a factor of ~ 2 at high z for some bursts.
3. This same effect can occasionally turn long GRBs into short GRBs.
4. Lastly, the simulated high- z sample is consistent with being drawn from the same population as the observed high- z sample, implying that observed high- z GRBs also suffer from underestimated duration and fluence measurements **that are found to occur in our simulations**.

In contrast to our results, O. M. Littlejohns et al. (2013) found a $\sim 1\%$ probability that the high- z GRB sample observed by Swift/BAT is drawn from the same population as the bright low- z sample, implying their simulated and observed samples are, at best, marginally consistent. One possibility is the difference in selected samples. O. M. Littlejohns et al. (2013) used a sample of 114 low-redshift GRBs for which the R. Willingale et al. (2010) pulse-fitting methodology had been applied, instead of the bright sample of bursts used in this work. Furthermore, there are differences in the methodologies used to perform the GRB simulations that could have lead to the inconsistency between the results. For example, O. M. Littlejohns et al. (2013) simulated a sample of bursts with measured redshifts $z < 4$ out to a single redshift value equal to that of the average redshift of their high- z sample, i.e., $\bar{z}_{\text{high}} = 7.66$. Further comparisons between the two methodologies will be needed to determine the cause of the inconsistent results.

Over its lifetime, Swift's average pointing interval has decreased, i.e., from ~ 990 sec in 2005 to ~ 650 sec in 2025. Recent studies of a potential class of ultra-long GRBs (i.e., GRBs with T_{90} s of a few thousand seconds or more; D. Gruber et al. 2011; B. Gendre et al.

2013; A. J. Levan et al. 2014; N. Dagoneau et al. 2020) have proposed that Swift's pointing strategy may bias against the discovery of GRBs with durations similar to or longer than the average pointing interval. From this work, we find that typical LGRBs are not observed as ultra-long GRBs at high redshifts. The only burst in our sample with simulation measurements of $T_{90} > 1,000$ seconds at $z = 9$ is GRB 130427A, which was an exceptionally bright GRB observed at a redshift of $z = 0.34$ and shows significant emission in BAT > 900 seconds after the initial trigger time. Therefore, if a population of ultra-long GRBs does exist at moderate- to high- redshifts, it would require an evolution in the γ -ray emission duration with redshift or, potentially, a unique progenitor system only present at those redshifts.

Studies of the tip-of-the-iceberg effect have investigated its effect on various duration measurement algorithm, e.g., Bayesian blocks, T_{90} , and T_{50} methods. Similar to the results of this work, it has been found that each duration estimator is affected by underestimation biases. Duration estimation algorithms that attempt to estimate the total length of emission, e.g., the Bayesian blocks and T_{100} methods, tend to be more strongly affected that more conservative duration estimations, e.g., the T_{50} (J. T. Bonnell et al. 1997; S. McBreen et al. 2002; D. Kocevski & V. Petrosian 2013). Using alternative duration measurement techniques, like only measuring the T_{90} of each isolated pulse in a GRB light curve, may lead to more consistent estimates of central engine lifetimes.

Our results imply that the measured duration of gamma-ray emission is not always an accurate estimation of the lifetime of GRB central engine activity due to instrumental bias (a result similarly found by M. Petropoulou et al. 2020). This claim is further supported by recent observations made by the Einstein Probe (EP), which has seen the X-ray emission of some GRBs lasting much longer than the gamma-ray emission observed by gamma-ray detectors such as Swift/BAT and Konus/Wind (Y. Liu et al. 2025; S.-Q. Jiang et al. 2025; D.-Y. Li et al. 2025). The difference in these duration measurements may not be physical but, instead, may simply be a reflection of the fact that the EP is a more sensitive all-sky monitor compared to our current soft gamma-ray instruments (see Extended Data Fig. 1 in Y. Liu et al. (2025); W. Yuan et al. 2022). More sensitive all-sky monitors that can detect the onset of the soft gamma-ray emission will be needed to truly constrain the lifetime of GRB central engines.

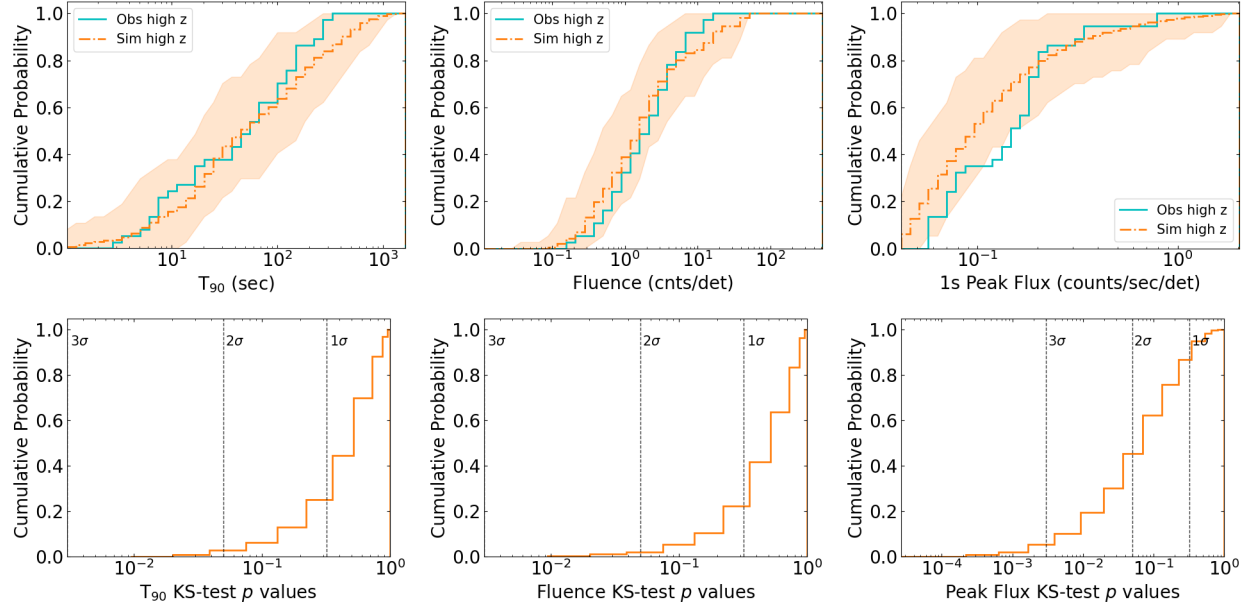


Figure 10. Same description as for Figure 9, but only using high- z bursts observed by Swift/BAT before January 1, 2012.

ACKNOWLEDGMENTS

MM's research was supported by an appointment to the NASA Postdoctoral Program at the NASA Goddard Space Flight Center, administered by Oak Ridge Associated Universities under contract with NASA.

Facilities: Swift(BAT)

Software: numpy (C. R. Harris et al. 2020), astropy (Astropy Collaboration et al. 2013, 2018, 2022), scipy (P. Virtanen et al. 2020)

DATA AVAILABILITY

All Swift/BAT GRB observations are publicly available in an online catalog <https://swift.gsfc.nasa.gov/>

REFERENCES

Abbott, B. P., Abbott, R., Abbott, T. D., et al. 2017, ApJL, 848, L13, doi: [10.3847/2041-8213/aa920c](https://doi.org/10.3847/2041-8213/aa920c)

Ahumada, T., Singer, L. P., Anand, S., et al. 2021, Nature Astronomy, 5, 917, doi: [10.1038/s41550-021-01428-7](https://doi.org/10.1038/s41550-021-01428-7)

Ajello, M., Arimoto, M., Axelsson, M., et al. 2019, ApJ, 878, 52, doi: [10.3847/1538-4357/ab1d4e](https://doi.org/10.3847/1538-4357/ab1d4e)

Astropy Collaboration, Robitaille, T. P., Tollerud, E. J., et al. 2013, A&A, 558, A33, doi: [10.1051/0004-6361/201322068](https://doi.org/10.1051/0004-6361/201322068)

Astropy Collaboration, Price-Whelan, A. M., Sipőcz, B. M., et al. 2018, AJ, 156, 123, doi: [10.3847/1538-3881/aabc4f](https://doi.org/10.3847/1538-3881/aabc4f)

Astropy Collaboration, Price-Whelan, A. M., Lim, P. L., et al. 2022, ApJ, 935, 167, doi: [10.3847/1538-4357/ac7c74](https://doi.org/10.3847/1538-4357/ac7c74)

Barthelmy, S. D., Barbier, L. M., Cummings, J. R., et al. 2005, SSRv, 120, 143, doi: [10.1007/s11214-005-5096-3](https://doi.org/10.1007/s11214-005-5096-3)

Baumgartner, W. H., Tueller, J., Markwardt, C. B., et al. 2013, ApJS, 207, 19, doi: [10.1088/0067-0049/207/2/19](https://doi.org/10.1088/0067-0049/207/2/19)

Blandford, R. D., & McKee, C. F. 1976, Physics of Fluids, 19, 1130, doi: [10.1063/1.861619](https://doi.org/10.1063/1.861619)

Bloom, J. S., Frail, D. A., & Sari, R. 2001, AJ, 121, 2879, doi: [10.1086/321093](https://doi.org/10.1086/321093)

Bonnell, J. T., Norris, J. P., Nemiroff, R. J., & Scargle, J. D. 1997, ApJ, 490, 79, doi: [10.1086/304841](https://doi.org/10.1086/304841)

Bromberg, O., Nakar, E., Piran, T., & Sari, R. 2012, ApJ, 749, 110, doi: [10.1088/0004-637X/749/2/110](https://doi.org/10.1088/0004-637X/749/2/110)

Cavallo, G., & Rees, M. J. 1978, MNRAS, 183, 359, doi: [10.1093/mnras/183.3.359](https://doi.org/10.1093/mnras/183.3.359)

Cucchiara, A., Levan, A. J., Fox, D. B., et al. 2011, ApJ, 736, 7, doi: [10.1088/0004-637X/736/1/7](https://doi.org/10.1088/0004-637X/736/1/7)

Dagoneau, N., Schanne, S., Atteia, J.-L., Götz, D., & Cordier, B. 2020, Experimental Astronomy, 50, 91, doi: [10.1007/s10686-020-09665-w](https://doi.org/10.1007/s10686-020-09665-w)

DeLaunay, J., & Tohuvavohu, A. 2022, ApJ, 941, 169, doi: [10.3847/1538-4357/ac9d38](https://doi.org/10.3847/1538-4357/ac9d38)

Fausey, H. M., Vejlgaard, S., van der Horst, A. J., et al. 2024, arXiv e-prints, arXiv:2403.13126, doi: [10.48550/arXiv.2403.13126](https://doi.org/10.48550/arXiv.2403.13126)

Fenimore, E. E., in 't Zand, J. J. M., Norris, J. P., Bonnell, J. T., & Nemiroff, R. J. 1995, ApJL, 448, L101, doi: [10.1086/309603](https://doi.org/10.1086/309603)

Frail, D. A., Waxman, E., & Kulkarni, S. R. 2000, ApJ, 537, 191, doi: [10.1086/309024](https://doi.org/10.1086/309024)

Galama, T. J., Vreeswijk, P. M., van Paradijs, J., et al. 1998, Nature, 395, 670, doi: [10.1038/27150](https://doi.org/10.1038/27150)

Galama, T. J., Vreeswijk, P. M., van Paradijs, J., et al. 1999, A&AS, 138, 465, doi: [10.1051/aas:1999311](https://doi.org/10.1051/aas:1999311)

Gendre, B., Stratta, G., Atteia, J. L., et al. 2013, ApJ, 766, 30, doi: [10.1088/0004-637X/766/1/30](https://doi.org/10.1088/0004-637X/766/1/30)

Gruber, D., Krühler, T., Foley, S., et al. 2011, A&A, 528, A15, doi: [10.1051/0004-6361/201015891](https://doi.org/10.1051/0004-6361/201015891)

Harris, C. R., Millman, K. J., van der Walt, S. J., et al. 2020, Nature, 585, 357, doi: [10.1038/s41586-020-2649-2](https://doi.org/10.1038/s41586-020-2649-2)

Hjorth, J., Sollerman, J., Møller, P., et al. 2003, Nature, 423, 847, doi: [10.1038/nature01750](https://doi.org/10.1038/nature01750)

Jiang, S.-Q., Xu, D., van Hoof, A. P. C., et al. 2025, ApJL, 988, L34, doi: [10.3847/2041-8213/addebf](https://doi.org/10.3847/2041-8213/addebf)

Kocevski, D., & Butler, N. 2008, ApJ, 680, 531, doi: [10.1086/586693](https://doi.org/10.1086/586693)

Kocevski, D., & Petrosian, V. 2013, ApJ, 765, 116, doi: [10.1088/0004-637X/765/2/116](https://doi.org/10.1088/0004-637X/765/2/116)

Kocevski, D., Ryde, F., & Liang, E. 2003, ApJ, 596, 389, doi: [10.1086/377707](https://doi.org/10.1086/377707)

Koshut, T. M., Kouveliotou, C., Paciesas, W. S., et al. 1995, ApJ, 452, 145, doi: [10.1086/176286](https://doi.org/10.1086/176286)

Kouveliotou, C., Meegan, C. A., Fishman, G. J., et al. 1993, ApJL, 413, L101, doi: [10.1086/186969](https://doi.org/10.1086/186969)

Levan, A. J., Tanvir, N. R., Starling, R. L. C., et al. 2014, ApJ, 781, 13, doi: [10.1088/0004-637X/781/1/13](https://doi.org/10.1088/0004-637X/781/1/13)

Levan, A. J., Gompertz, B. P., Salafia, O. S., et al. 2024, Nature, 626, 737, doi: [10.1038/s41586-023-06759-1](https://doi.org/10.1038/s41586-023-06759-1)

Li, D.-Y., Zhang, W.-D., Yang, J., et al. 2025, arXiv e-prints, arXiv:2509.25877, doi: [10.48550/arXiv.2509.25877](https://doi.org/10.48550/arXiv.2509.25877)

Lien, A., Sakamoto, T., Barthelmy, S. D., et al. 2016, ApJ, 829, 7, doi: [10.3847/0004-637X/829/1/7](https://doi.org/10.3847/0004-637X/829/1/7)

Littlejohns, O. M., Tanvir, N. R., Willingale, R., et al. 2013, MNRAS, 436, 3640, doi: [10.1093/mnras/stt1841](https://doi.org/10.1093/mnras/stt1841)

Liu, Y., Sun, H., Xu, D., et al. 2025, Nature Astronomy, doi: [10.1038/s41550-024-02449-8](https://doi.org/10.1038/s41550-024-02449-8)

Llamas Lanza, M., Godet, O., Arcier, B., et al. 2024, arXiv e-prints, arXiv:2403.03266, doi: [10.48550/arXiv.2403.03266](https://doi.org/10.48550/arXiv.2403.03266)

Mao, S., & Mo, H. J. 1998, A&A, 339, L1, doi: [10.48550/arXiv.astro-ph/9808342](https://doi.org/10.48550/arXiv.astro-ph/9808342)

McBreen, S., McBreen, B., Hanlon, L., & Quilligan, F. 2002, A&A, 393, L29, doi: [10.1051/0004-6361:20021073](https://doi.org/10.1051/0004-6361:20021073)

Miralda-Escudé, J. 1998, ApJ, 501, 15, doi: [10.1086/305799](https://doi.org/10.1086/305799)

Moss, M., Lien, A., Guiriec, S., Cenko, S. B., & Sakamoto, T. 2022, ApJ, 927, 157, doi: [10.3847/1538-4357/ac4d94](https://doi.org/10.3847/1538-4357/ac4d94)

Murakami, T., Inoue, H., Nishimura, J., van Paradijs, J., & Fenimore, E. E. 1991, Nature, 350, 592, doi: [10.1038/350592a0](https://doi.org/10.1038/350592a0)

Nysewander, M., Fruchter, A. S., & Pe'er, A. 2009, ApJ, 701, 824, doi: [10.1088/0004-637X/701/1/824](https://doi.org/10.1088/0004-637X/701/1/824)

Petropoulou, M., Beniamini, P., Vasilopoulos, G., Giannios, D., & Barniol Duran, R. 2020, MNRAS, 496, 2910, doi: [10.1093/mnras/staa1695](https://doi.org/10.1093/mnras/staa1695)

Planck Collaboration, Aghanim, N., Akrami, Y., et al. 2020, A&A, 641, A6, doi: [10.1051/0004-6361/201833910](https://doi.org/10.1051/0004-6361/201833910)

Porciani, C., & Madau, P. 2001, ApJ, 548, 522, doi: [10.1086/319027](https://doi.org/10.1086/319027)

Rastinejad, J. C., Gompertz, B. P., Levan, A. J., et al. 2022, Nature, 612, 223, doi: [10.1038/s41586-022-05390-w](https://doi.org/10.1038/s41586-022-05390-w)

Rees, M. J., & Meszaros, P. 1992, MNRAS, 258, 41, doi: [10.1093/mnras/258.1.41P](https://doi.org/10.1093/mnras/258.1.41P)

Rossi, A., Rothberg, B., Palazzi, E., et al. 2022, ApJ, 932, 1, doi: [10.3847/1538-4357/ac60a2](https://doi.org/10.3847/1538-4357/ac60a2)

Salvaterra, R., Campana, S., Vergani, S. D., et al. 2012, ApJ, 749, 68, doi: [10.1088/0004-637X/749/1/68](https://doi.org/10.1088/0004-637X/749/1/68)

Sari, R., Piran, T., & Narayan, R. 1998, ApJL, 497, L17, doi: [10.1086/311269](https://doi.org/10.1086/311269)

Scargle, J. D., Norris, J. P., Jackson, B., & Chiang, J. 2013, ApJ, 764, 167, doi: [10.1088/0004-637X/764/2/167](https://doi.org/10.1088/0004-637X/764/2/167)

Selsing, J., Malesani, D., Goldoni, P., et al. 2019, A&A, 623, A92, doi: [10.1051/0004-6361/201832835](https://doi.org/10.1051/0004-6361/201832835)

Skinner, G. K. 2008, Applied Optics, 47, 2739, doi: [10.1364/AO.47.002739](https://doi.org/10.1364/AO.47.002739)

Stanek, K. Z., Matheson, T., Garnavich, P. M., et al. 2003, ApJL, 591, L17, doi: [10.1086/376976](https://doi.org/10.1086/376976)

Tanvir, N. R., Levan, A. J., Fruchter, A. S., et al. 2013, Nature, 500, 547, doi: [10.1038/nature12505](https://doi.org/10.1038/nature12505)

Tanvir, N. R., Fynbo, J. P. U., de Ugarte Postigo, A., et al. 2019, MNRAS, 483, 5380, doi: [10.1093/mnras/sty3460](https://doi.org/10.1093/mnras/sty3460)

Totani, T. 1997, ApJL, 486, L71, doi: [10.1086/310853](https://doi.org/10.1086/310853)

Totani, T., Kawai, N., Kosugi, G., et al. 2006, PASJ, 58, 485, doi: [10.1093/pasj/58.3.485](https://doi.org/10.1093/pasj/58.3.485)

Troja, E., Rosswog, S., & Gehrels, N. 2010, ApJ, 723, 1711, doi: [10.1088/0004-637X/723/2/1711](https://doi.org/10.1088/0004-637X/723/2/1711)

Troja, E., Fryer, C. L., O'Connor, B., et al. 2022, Nature, 612, 228, doi: [10.1038/s41586-022-05327-3](https://doi.org/10.1038/s41586-022-05327-3)

Ukwatta, T. N., Barthelmy, S. D., Evans, P. A., et al. 2009, GRB Coordinates Network, 9281, 1

Virtanen, P., Gommers, R., Oliphant, T. E., et al. 2020, Nature Methods, 17, 261, doi: [10.1038/s41592-019-0686-2](https://doi.org/10.1038/s41592-019-0686-2)

Wijers, R. A. M. J., Bloom, J. S., Bagla, J. S., & Natarajan, P. 1998, MNRAS, 294, L13, doi: [10.1046/j.1365-8711.1998.01328.x](https://doi.org/10.1046/j.1365-8711.1998.01328.x)

Wijers, R. A. M. J., Rees, M. J., & Meszaros, P. 1997, MNRAS, 288, L51, doi: [10.1093/mnras/288.4.L51](https://doi.org/10.1093/mnras/288.4.L51)

Willingale, R., Genet, F., Granot, J., & O'Brien, P. T. 2010, MNRAS, 403, 1296, doi: [10.1111/j.1365-2966.2009.16187.x](https://doi.org/10.1111/j.1365-2966.2009.16187.x)

Yonetoku, D., Murakami, T., Nakamura, T., et al. 2004, ApJ, 609, 935, doi: [10.1086/421285](https://doi.org/10.1086/421285)

Yuan, W., Zhang, C., Chen, Y., & Ling, Z. 2022, in Handbook of X-ray and Gamma-ray Astrophysics, ed. C. Bambi & A. Sanganello, 86, doi: [10.1007/978-981-16-4544-0_151-1](https://doi.org/10.1007/978-981-16-4544-0_151-1)

Zhang, B. 2014, International Journal of Modern Physics D, 23, 1430002, doi: [10.1142/S021827181430002X](https://doi.org/10.1142/S021827181430002X)

Table 3. p -values obtained from KS-tests performed between Swift/BAT GRBs observed before and after 2012-01-01

Metric	p -value	Significance
Durations	0.61	$< 1\sigma$
Fluences	0.24	$< 2\sigma$
Peak Flux	0.05	$= 2\sigma$

APPENDIX

A. EXCLUDING LATE-MISSION GRBS

In Figure 11 measurements of the pre-2012 and post-2012 samples are compared to one another and the respective KS-Test p -values calculated between the distributions are given in Table 3. We can see that duration measurements of the pre-2012 and post-2012 samples are consistent with one another to within 1σ (i.e., $p = 0.61$), however, the fluence measurements of the two samples are only consistent within 2σ (i.e., $p = 0.24$) and the peak flux measurements are only just barely consistent at 2σ (i.e., $p = 0.05$). Naively, since these are all high- z GRBs, these measurements are drawn from the same underlying distribution and a KS-Test should find $p \geq 0.32$ to indicate this fact. However, there is not a $> 3\sigma$ difference between any of sample measurements so we cannot claim that the samples are being drawn from different distributions either.

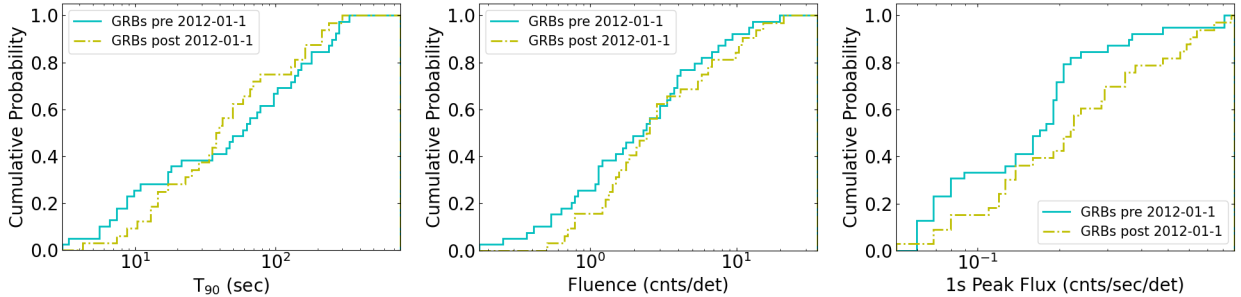


Figure 11. Displayed are the cumulative distributions of the measured durations (*Top*), fluences (*Center*), and peak fluxes (*Bottom*) for Swift/BAT GRBs observed before 2012-01-01 (cyan) and those observed after (olive). The p -values obtained from KS-tests for these distributions can be found in Table

We separated our observed high- z GRB sample into GRBs observed before and after 2012-01-01, however, that date was simply an initial guess. We were not sure what date would be appropriate to make a cut at or even if an evolving bias was truly present at all. To investigate if there was any evolving bias in Swift/BAT GRBs and what date it may have become significant, we first looked into the average peak flux of Swift/BAT GRBs over the course of the mission’s life (see Fig. 12 *a*). There seems to be a slight increase in the average peak flux for the entire Swift/BAT GRB sample, however this increase is less than a factor of 2. Looking only at Swift/BAT GRBs that have measured redshifts, it seems this peak-flux increase may be more pronounced (see Fig. 12 *b*). For GRBs with redshifts $z > 3$, this bias does not seem to be present, but the sample size is quite low, especially so after 2016 (see Fig. 12 *c*). But even for GRBs without any redshifts, there seems to be a slight increase in the peak flux (see Fig. 12 *d*). From this comparison, it looks as if $z > 3$ GRBs actually stick close to the same average peak flux across the mission life time and that there is a possible increase in the average peak flux for $z < 3$ GRBs.

This change in average peak flux could be due to a number of reasons. For instance, it may be due to the decrease in the number of active detectors on the BAT detector plane (see Fig. 13). The sensitivity of BAT goes as $\propto \sqrt{N}$,

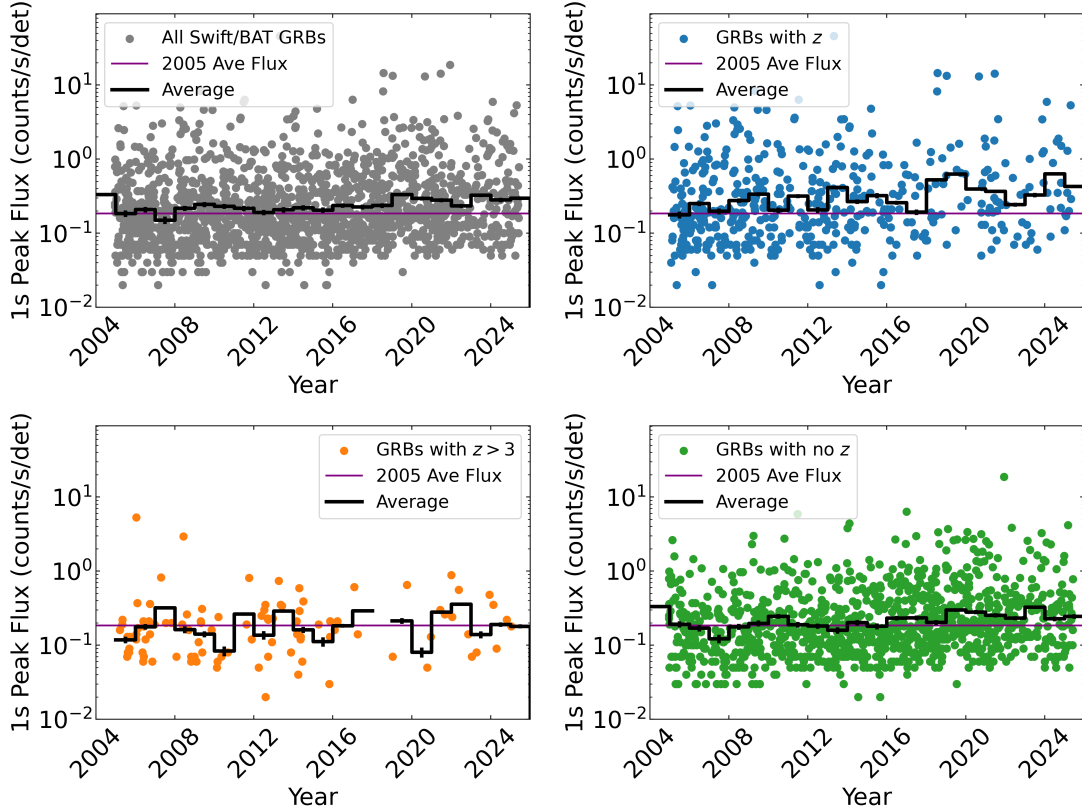


Figure 12. Displayed are the 1-second peak fluxes for *a*: all Swift/BAT GRBs, *b*: only GRBs with redshifts, *c*: only GRBs with redshifts $z > 3$, and *d*: only GRBs without redshifts as a function of their observation date. The average peak flux in 6-month bins is shown with the solid lines in each plot. The thin purple line indicates the 2005 average peak flux.

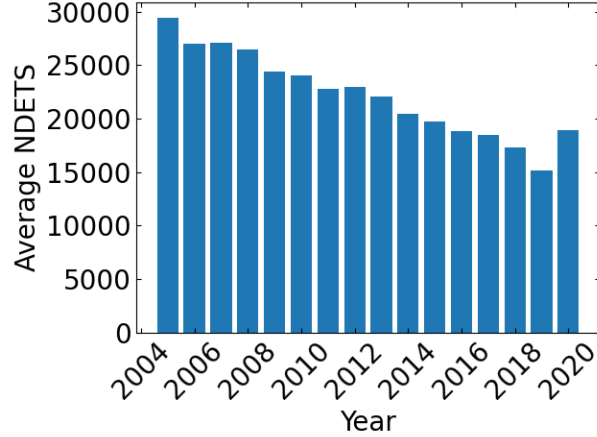


Figure 13. Average number of enabled/active detectors on the Swift/BAT detector plane. The total number of detectors at launch was 32,768. In early 2020, BAT recovered a significant number of detectors upon a spontaneous reboot.

where N is the number of detectors active on the detector plane (G. K. Skinner 2008; W. H. Baumgartner et al. 2013). The ratio between the number of active detectors on BAT at the beginning of Swift's lifetime (i.e., $N_0 = 32,768$) and the average number of active detectors in 2018 (i.e., $N_{18} \sim 15,000$) equates to $\sqrt{N_{18}/N_0} = 0.676$, indicating that the sensitivity of BAT is expected to have decreased by $\sim 33\%$ between 2004 and 2018.

An alternative cause of the average peak flux change could be due an evolution in Swift's observing strategy; over Swift's lifetime, its average pointing interval has decreased from ~ 990 sec in 2005 to ~ 650 sec in 2025 and, consequently,

its time spent slewing between pointings has increased. During a slew, Swift does not trigger and becomes less sensitive to dim and short events.

Lastly, over the last two decades, the fraction of GRBs observed by Swift that obtain redshift measurements from ground-based follow-up has decreased, leading to a lower redshift completeness and, possibly, also leading to some population bias (see Fig. 14 *Left*). M. Nysewander et al. (2009) found that a positive correlation exists for GRBs between their measured prompt emission fluence and their optical afterglow brightness measured after 11 hours, so it may be the case that ground-based facilities are choosing to perform follow-up observations of only GRBs with high-fluence prompt emission or, perhaps, performing less deep follow-up observations each year, leading to redshift measurements being obtained only for those GRBs with brighter afterglows and, consequently, higher fluence prompt emission. This could lead to either (i) an increase in the peak flux of high- z GRBs – since there exists a strong correlation that exists between GRB peak fluxes and fluences (M. Ajello et al. 2019) – however, Figure 12 doesn’t show any average increase for high- z GRBs, or (ii) a decrease in the average redshift for Swift/BAT GRBs over time. In Figure 14 *Middle*, we show the average redshift of Swift/BAT triggered GRBs over time and find a possible small decrease of the average redshift starting in \sim 2016, however the averages in 2022 and 2024 don’t support this trend (although they are statistically limited). A KS-Test between the redshift distributions of the pre- and post- 2012 GRBs obtains $p = 0.71$, meaning they are not incompatible with coming from the same underlying distribution (see Fig. 14 *Right*).

Although there are hints to an emerging bias, a conclusive answer on whether there is a bias developing for Swift/BAT GRBs, either due to BAT sensitivity degrading or observational strategies, may be difficult to uncover and is outside the scope of this work.

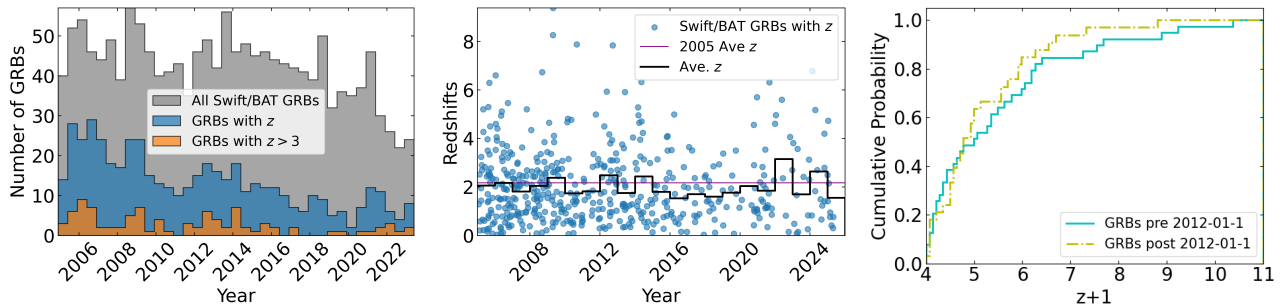


Figure 14. *Left:* The number of redshift measurements obtained for Swift/BAT GRBs as a function of date since mission launch. All Swift/BAT GRBs are shown in gray, Swift/BAT GRBs with redshift in blue, and GRBs with redshifts $z > 3$ in orange. *Middle:* The average redshift measured for Swift/BAT GRBs as a function of their observation date. Swift/BAT GRBs are displayed in blue point. The black line indicates the average redshift since Swift’s launch. Again, the thin purple line is just an extrapolation of the the 2005 average. *Right:* Cumulative redshift distribution for GRBs observed before 2012-01-01 and those observed after. A KS-test performed between the two distributions obtains a p -value = 0.71, indicating that they are not incompatible with being drawn from the same distribution.

Table 4. GRBs in our low- z sample (i.e., $z < 1$)

GRB Name	z	$T_{90,\text{true}}$ (sec)	Fluence (cnts/det)	α	E_p (keV)	N_0 (cnts $\text{cm}^{-2} \text{s}^{-1} \text{keV}^{-1}$)
050525A	0.606	8.836	25.619	-0.603	106.319	0.776
060904B	0.7029	189.98	2.926	-1.061	342.243	0.024
060912A	0.937	5.028	2.253	-1.196	86.386	0.112
070508	0.82	20.9	29.116	-0.679	213.491	0.307
071010B	0.947	36.124	8.2	-1.001	68.532	0.133
090424	0.544	49.46	33.035	-0.984	183.397	0.826
090510	0.903	5.664	0.846	-0.567	264.487	0.053
090618	0.54	113.34	177.209	-1.235	364.469	0.363
091018	0.971	4.368	3.092	-1.298	35.062	0.191
091127	0.49044	6.956	13.548	-1.33	69.588	0.575
100621A	0.542	63.552	38.87	-0.946	90.632	0.202
100816A	0.8049	2.884	2.693	-0.494	153.042	0.171
110715A	0.8224	13.0	18.701	-0.985	151.992	0.656
111228A	0.71627	101.244	16.039	-1.644	93.714	0.109
120907A	0.97	6.08	0.954	-1.301	411.019	0.026
130427A	0.3399	244.332	520.716	-0.502	467.392	3.771
130831A	0.4791	30.192	10.745	-1.545	149.325	0.122
140506A	0.889	111.104	4.09	-0.53	100.377	0.217
140512A	0.725	154.112	20.406	-1.007	224.843	0.066
161001A	0.891	2.6	0.978	-0.572	375.703	0.037
180720B	0.654	108.4	121.571	-0.664	214.739	0.853
201024A	0.999	5.0	1.5	-1.832	25.887	0.034
210104A	0.92	32.048	14.183	-1.047	164.371	0.136
231118A	0.8304	151.488	6.339	-0.606	145.042	0.146
240205B	0.824	47.304	54.371	-1.161	118.838	0.571
250424A	0.31	18.632	51.953	-1.336	145.293	0.481

B. DATA TABLES

In Tables 4 and 5 we display the samples of observed low- z and high- z GRBs are listed, respectively. These samples are both taken from a redshift complete sample of GRBs observed with the VLT/X-shooter (J. Selsing et al. 2019), but includes a further cut of a 1-s peak flux $f_p \geq 2.6 \text{ counts s}^{-1} \text{ cm}^{-2}$ in order to more closely follow the BAT6 sample (R. Salvaterra et al. 2012).

Fig. Set 1. Low- z GRB Light Curves and Simulation Results

Table 5. GRBs in our high- z sample (i.e., $z > 3$)

GRB Name	z	$T_{90,\text{true}}$	Fluence
		(sec)	(cnts/det)
050319	3.2425	151.584	2.432
050502B	5.2	17.724	0.822
050505	4.2748	58.852	3.422
050814	5.3	142.852	3.06
050904	6.295	181.576	7.806
050908	3.3467	18.284	0.85
050922B	4.5	157.024	4.252
060116	6.6	104.832	3.579
060206	4.0559	7.552	1.559
060223A	4.41	11.32	1.099
060522	5.11	69.124	1.753
060526	3.2213	298.04	2.603
060605	3.773	79.84	1.228
060607A	3.0749	103.032	4.069
060906	3.6856	44.588	3.863
060926	3.2086	8.824	0.56
060927	5.4636	22.416	2.002
061110B	3.4344	135.248	1.845
061222B	3.355	37.248	4.041
070420	3.01	77.024	20.501
070721B	3.6298	336.864	5.194
071025	5.2	241.296	12.647
080129	4.349	50.18	1.176
080516	3.2	5.764	0.422
080913	6.733	7.456	0.766
081028A	3.038	284.424	6.964
081029	3.8479	275.104	3.158
081228	3.44	3.0	0.173
090205	4.6497	8.812	0.387
090423	8.26	10.304	1.19
090429B	9.38	5.58	0.645
090516A	4.109	181.008	13.275
090715B	3.0	266.4	9.744
091109A	3.076	48.032	2.354
100302A	4.813	17.948	0.557
100316A	3.155	6.752	1.181
100905A	7.88	3.396	0.255
110818A	3.36	102.84	5.988
111008A	4.99005	62.848	8.51

Table 6. Continued: GRBs in our high- z sample (i.e., $z > 3$)

GRB Name	z	$T_{90,\text{true}}$	Fluence
		(sec)	(cnts/det)
120712A	4.1745	14.808	2.685
120802A	3.796	50.288	2.911
120909A	3.93	220.596	11.349
120922A	3.1	168.224	9.912
120923A	7.84	26.076	0.687
121201A	3.385	38.0	1.399
121217A	3.1	778.092	10.497
130408A	3.758	4.24	2.226
130514A	3.6	214.192	15.499
131117A	4.042	10.88	0.528
140114A	3.0	139.948	6.482
140304A	5.283	14.784	1.659
140311A	4.954	70.48	3.372
140419A	3.956	80.076	21.973
140423A	3.26	134.144	14.079
140515A	6.33	23.416	1.253
140518A	4.707	60.524	2.114
140703A	3.14	68.644	5.917
150413A	3.139	243.596	6.824
160203A	3.52	17.44	1.788
160327A	4.99	33.744	2.509
170202A	3.645	37.76	5.6
191004B	3.503	300.128	4.383
201014A	4.56	36.196	0.706
201221A	5.7	44.316	2.699
210610A	3.54	13.616	1.55
220101A	4.61	161.888	35.848
220117A	4.961	50.56	2.974
220521A	5.6	13.548	1.46
221110A	4.06	8.98	0.798
230116D	3.81	41.0	1.332
230414B	3.568	29.06	0.82
231210B	3.13	7.472	1.921